

Third order optical nonlinearity of three dimensional massless Dirac fermions

J. L. Cheng,^{1,2,*} J. E. Sipe,³ and S. W. Wu⁴

¹*The Guo China-US Photonics Laboratory,
State Key Laboratory of Applied Optics,
Changchun Institute of Optics, Fine Mechanics and Physics,
Chinese Academy of Sciences, Changchun 130033, China.*

²*School of Physical Sciences, University of Chinese
Academy of Sciences, Beijing 100049, China*

³*Department of Physics, University of Toronto, Toronto, Ontario, Canada*

⁴*State Key Laboratory of Surface Physics,
Key Laboratory of Micro and Nano Photonic Structures (MOE),
and Department of Physics, Fudan University, Shanghai 200433, China*

Abstract

We present analytic expressions for the electronic contributions to the linear conductivity $\sigma_{3d}^{(1)}(\omega)$ and the third order optical conductivity $\sigma_{3d}^{(3)}(\omega_1, \omega_2, \omega_3)$ of three dimensional massless Dirac fermions, the quasi-particles relevant for the low energy excitation of topological Dirac semimetals and Weyl semimetals. Although there is no gap for massless Dirac fermions, a finite chemical potential μ can lead to an effective gap parameter, which plays an important role in the qualitative features of interband optical transitions. For gapless linear dispersion in three dimension, the imaginary part of the linear conductivity diverges as a logarithmic function of the cutoff energy, while the real part is linear with photon frequency ω as $\hbar\omega > 2|\mu|$. The third order conductivity exhibits features very similar to those of two dimensional Dirac fermions, *i.e.*, graphene, but with the amplitude for a single Dirac cone generally two orders of magnitude smaller in three dimension than in two dimension. There are many resonances associated with the chemical potential induced gap parameters, and divergences associated with the intraband transitions. The details of the third order conductivity are discussed for third harmonic generation, the Kerr effect and two-photon carrier injection, parametric frequency conversion, and two-color coherent current injection. Although the expressions we derive are limited to the clean limit at zero temperature, the generalization to include phenomenological relaxation processes at finite temperature is straightforward and is presented.

I. INTRODUCTION

Two dimensional (2D) massless Dirac fermions (DFs) have been investigated extensively in condensed matter systems since their first experimental realization in graphene, and their properties are significantly different than those of fermions in the more usual parabolic bands.^{1,2} Their attractive optical properties³ include broadband linear optical absorption and the ability to use the chemical potential to tune both plasmon resonances and an extremely strong nonlinear optical response.⁴ The strong nonlinear response makes graphene a potential candidate for integration in photonic devices⁵⁻⁷ as a source of nonlinear functionality, and it has been the focus of a large number of experimental^{8,9} and theoretical¹⁰⁻¹⁸ studies over the past decade. Experiments have explored different nonlinear phenomena including third harmonic generation (THG), the Kerr effect and two photon carrier injection, parametric frequency conversion (PFC), and two-color coherent current injection (CCI); the corresponding nonlinear coefficients have been extracted for different photon energies and chemical potentials. Theoretical studies have been mainly at the level of independent particle approximation, and have presented perturbative expressions and numerical simulations. Recently, many-body effects¹⁹⁻²¹ have been shown to play a significant role in the nonlinear optical response. And in the development of theories of topological materials, 2D massless DFs have been shown to determine the properties of the low energy excitation of surface states of a topological insulators, despite the small energy range over which the linear dispersion approximation is valid.

In a two band model for 2D DFs, a mass can be introduced. The resulting dispersion relation can be realized around the band edge of gapped graphene, or around the band edge of a monolayer of BN or MoS₂, and in other 2D materials. The optical nonlinearities of 2D massive DFs have also been investigated both experimentally and theoretically. Jafari²² presented a theory for THG using a Feynman diagrammatic technique, describing the light-matter interaction in the framework of a vector potential. However, in the limit of vanishing mass his result does not converge to the results of other studies.¹¹ Cheng *et al.* investigated various nonlinear effects both by numerically solving the equations of motion¹³ and by approximation from the results of gapped graphene under a perpendicular magnetic field.²³ Recently, we derived analytic expressions for the third order conductivities of gapped graphene²⁴ at general frequencies, following earlier work on graphene.¹²

There have also been a host of recent studies focused on the prediction and discovery of *three* dimensional (3D) Dirac and Weyl semimetals,^{25–32} where the low energy excitations can be described by DFs with a *three* dimensional wave vector. As an analogue of 2D massless DFs, 3D massless DFs³² possess gapless linear dispersion and an interesting band topology around the Dirac point, which leads to extraordinary optical properties. As well, the chiral anomaly in Weyl semimetals can be probed with the presence of both the electric field and magnetic field.³³ The nonlinear optical properties of 3D massless DFs have also attracted attention.^{34–40} Experimentally, huge nonlinear optical coefficients⁴¹ have been observed, although probably at frequencies much higher than those at which the linear dispersion approximation is valid. There are interesting recent theoretical predictions^{42–44} for the Kerr effect and THG, both within the framework of the Boltzmann equation and in a treatment including intraband and interband transitions. In these studies the focus was on frequencies in the terahertz regime, and possible applications in terahertz plasmonics have been investigated.⁴⁵ However, the light-matter interaction was described in a velocity gauge, and additional care may be required to confirm that no unphysical divergences have been induced by band truncation; a treatment based on the length gauge,^{46,47} where such difficulties are not present, is clearly in order. Further, in order to extend the application of these materials to various nonlinear optical scenarios, it would be helpful to understand the general frequency dependence of the third order conductivity, especially in a comparison with that of graphene; this has not yet been done.

In this work, we derive analytic expressions for linear and third order optical conductivities of 3D massless DFs. Our strategy is based on employing earlier results found for the linear and nonlinear optical response of gapped graphene. In fact, we show that the response coefficients for 3D massless DFs can be written as an integral over the results for gapped graphene with different gaps. Our treatment includes the intraband and interband optical transitions, in a framework where the light-matter interaction is described in the length gauge. Our expressions for the third order conductivities describe a general input frequency dependence for the clean limit at zero temperature. After analyzing the structures of the conductivities, we discuss in detail the coefficients for THG, the Kerr effect and two photon carrier injection, PFC, and two-color CCI. To better understand of the physics of the nonlinear processes, comparisons with that of graphene are made.

We organize the paper as following: in Section II we summarize the symmetries of fre-

quency dependence of the linear and nonlinear conductivities of 2D massive DFs. In Section III we describe how to construct the conductivity of 3D massless DFs from the conductivity of 2D massive DFs, and present the analytic expressions for linear conductivity and third order conductivity; in Section IV we discuss the details of the conductivities for different optical phenomena, including the linear optical response, THG, the Kerr effect and two photon carrier injection, PFC, and two-color CCI; in Sec. V we discuss and conclude, indicating how the extension of our results to include finite temperature and a phenomenological description of relaxation processes can easily be implemented.

II. CONDUCTIVITIES FOR 2D DIRAC FERMIONS

Two dimensional massive DFs in one Dirac cone can be described by the Hamiltonian

$$H_{2d}(\boldsymbol{\kappa}, \Delta) = \hbar v_F \boldsymbol{\kappa} \cdot \boldsymbol{\sigma} + \Delta \sigma_z. \quad (1)$$

where v_F is the Fermi velocity, $\boldsymbol{\sigma} = \sigma_x \hat{\boldsymbol{x}} + \sigma_y \hat{\boldsymbol{y}} + \sigma_z \hat{\boldsymbol{z}}$ has its components as Pauli matrices, $\boldsymbol{\kappa} = \kappa_x \hat{\boldsymbol{x}} + \kappa_y \hat{\boldsymbol{y}}$ is a two-dimensional wave vector, and Δ is a mass parameter to give a gap $2|\Delta|$ at the Dirac point. Depending on the material, there can exist multiple Dirac cones, and for different materials the model Hamiltonian can take in different forms. For example, the low energy excitations of gapped graphene are described by the Hamiltonian

$$H_{gg;\tau}(\boldsymbol{\kappa}, \Delta) = \hbar v_F (\tau \kappa_y \sigma_x - \kappa_x \sigma_y) + \Delta \sigma_z, \quad (2)$$

where $\tau = \pm$ is a valley index for two different Dirac cones.

For such Hamiltonians, we consider the linear optical conductivity tensor $\sigma^{(1);da}(\omega)$ and third order optical conductivity tensor $\sigma^{(3);dabc}(\omega_1, \omega_2, \omega_3)$, where the Roman letters d, a, b, c refer to the Cartesian directions, and ω and ω_i refer to the optical frequencies. The second order response vanishes in the dipole approximation, as we discuss below. The results of gapped graphene have been given earlier,²⁴ and will be summarized in the following.

A. Symmetry properties of conductivities for two dimensional massive Dirac fermions

We denote the conductivities for a 2D Dirac cone by $\sigma_{2d}^{(1);da}(\omega)$ and $\sigma_{2d}^{(3);dabc}(\omega_1, \omega_2, \omega_3)$. The Hamiltonian $H_{2d}(\boldsymbol{\kappa}, \Delta)$ satisfies the rotational symmetry condition

$$U_\theta H_{2d}(R_\theta \boldsymbol{\kappa}, \Delta) U_\theta^\dagger = H_{2d}(\boldsymbol{\kappa}, \Delta), \quad (3)$$

where θ is a rotation angle about the z axis, $U_\theta = \cos \frac{\theta}{2} - i \sin \frac{\theta}{2} \sigma_z$ is a unitary transformation acting on the spinors, and $R_\theta = \begin{pmatrix} \cos \theta & \sin \theta \\ -\sin \theta & \cos \theta \end{pmatrix}$ is rotation operation acting on $\boldsymbol{\kappa}$. The rotational symmetry determines that the linear conductivity includes only two independent components, *i.e.*, the diagonal component $\sigma_{2d}^{(1);xx}$ and the off-diagonal component $\sigma_{2d}^{(1);xy}$. The other nonzero components can be found from

$$\sigma_{2d}^{(1);xx} = \sigma_{2d}^{(1);yy}, \quad \sigma_{2d}^{(1);xy} = -\sigma_{2d}^{(1);yx}. \quad (4)$$

The off-diagonal components are nonzero because the Berry curvature at the Dirac point behaves as the vector potential of a magnetic monopole, and can contribute to a Hall conductivity. For the third order conductivity, there are in all six independent nonzero components, which can be taken to be $\sigma_{2d}^{(3);xxyy}$, $\sigma_{2d}^{(3);xyxy}$, $\sigma_{2d}^{(3);xyyx}$, $\sigma_{2d}^{(3);yyxy}$, $\sigma_{2d}^{(3);yyyx}$, and $\sigma_{2d}^{(3);yyyy}$. The other nonzero components are then given by

$$\sigma_{2d}^{(3);xxxx} = \sigma_{2d}^{(3);xxyy} + \sigma_{2d}^{(3);xyxy} + \sigma_{2d}^{(3);xyyx}, \quad (5)$$

$$\sigma_{2d}^{(3);yxxx} = \sigma_{2d}^{(3);yyxy} + \sigma_{2d}^{(3);yyyx} + \sigma_{2d}^{(3);yyyy}, \quad (6)$$

and

$$\sigma_{2d}^{(3);xxxx} = \sigma_{2d}^{(3);yyyy}, \quad \sigma_{2d}^{(3);yxxx} = -\sigma_{2d}^{(3);xyyy}, \quad (7)$$

$$\sigma_{2d}^{(3);xxyy} = \sigma_{2d}^{(3);yyxx}, \quad \sigma_{2d}^{(3);yyxy} = -\sigma_{2d}^{(3);xyxx}, \quad (8)$$

$$\sigma_{2d}^{(3);xyxy} = \sigma_{2d}^{(3);yxxy}, \quad \sigma_{2d}^{(3);yyyx} = -\sigma_{2d}^{(3);xxyx}, \quad (9)$$

$$\sigma_{2d}^{(3);xyyx} = \sigma_{2d}^{(3);yxxy}, \quad \sigma_{2d}^{(3);yyyy} = -\sigma_{2d}^{(3);xxxx}. \quad (10)$$

For a single Dirac cone, the independent components $\sigma_{2d}^{(1);xy}$, $\sigma_{2d}^{(3);xxyy}$, $\sigma_{2d}^{(3);yyxy}$, and $\sigma_{2d}^{(3);yyyx}$ are antisymmetric with respect to $\{x \leftrightarrow y\}$, while the others, $\sigma_{2d}^{(1);xx}$, $\sigma_{2d}^{(3);xxyy}$, $\sigma_{2d}^{(3);xyxy}$,

and $\sigma_{2d}^{(3);xyyx}$ are symmetric; we refer to these two different classes of tensor components as “antisymmetric” and “symmetric” components, respectively. Due to inversion symmetry

$$\sigma_z H_{2d}(-\boldsymbol{\kappa}, \Delta) \sigma_z = H_{2d}(\boldsymbol{\kappa}, \Delta), \quad (11)$$

and there is no second order response in the dipole approximation.

For 2D DFs, the sign of the mass parameter determines the chirality, and the two different possibilities are connected through

$$U_m H_{2d}(R_m \boldsymbol{\kappa}, \Delta) U_m^\dagger = H_{2d}(\boldsymbol{\kappa}, -\Delta), \quad (12)$$

with $U_m = \frac{i}{\sqrt{2}}(\sigma_x - \sigma_y)$ and $R_i = \begin{pmatrix} 0 & -1 \\ -1 & 0 \end{pmatrix}$. This relation gives $\sigma_{2d}^{(n);dab\dots}(-\Delta) = \sigma_{2d}^{(n);\bar{d}\bar{a}\bar{b}\dots}(\Delta)$ where the bar of a Roman letter means $\bar{d} = y, x$ for $d = x, y$. Furthermore, utilizing the consequences of rotational symmetry, we find that all symmetric (antisymmetric) components are even (odd) functions of Δ .

B. Conductivities of gapped graphene

We denote the conductivities that follow from the Hamiltonian $H_{gg;\tau}$ by $\sigma_{gg;\tau}^{(1);da}(\omega)$ and $\sigma_{gg;\tau}^{(3);dabc}(\omega_1, \omega_2, \omega_3)$. In the τ valley, the Hamiltonian connects to $H_{2d}(\boldsymbol{\kappa}, \Delta)$ through

$$H_{gg;\tau}(\boldsymbol{\kappa}, \Delta) = H_{2d}(R_\tau \boldsymbol{\kappa}, \Delta), \quad (13)$$

with an orthogonal matrix $R_\tau = \begin{pmatrix} 0 & \tau \\ -1 & 0 \end{pmatrix}$. From Eq. (13), the symmetric components satisfy $\sigma_{gg;\tau}^{(n);da\dots}(\Delta) = \sigma_{2d}^{(n);\bar{d}\bar{a}\dots}(\Delta)$, and antisymmetric components satisfy $\sigma_{gg;\tau}^{(n);da\dots}(\Delta) = \tau \sigma_{2d}^{(1);\bar{d}\bar{a}\dots}(\Delta)$. Therefore, for gapped graphene only the symmetric components survive, and they are

$$\sigma_{gg}^{(1);xx}(\omega) = 2 \sum_{\tau} \sigma_{gg;\tau}^{(1);xx}(\omega) = 4 \sigma_{2d}^{(1);xx}(\omega), \quad (14)$$

where the prefactor 2 comes from the spin degeneracy in gapped graphene. Similarly the third order conductivities are

$$\sigma_{gg}^{(3);dabc}(\omega_1, \omega_2, \omega_3) = 4 \sigma_{2d}^{(3);dabc}(\omega_1, \omega_2, \omega_3), \quad (15)$$

for $dabc = xxyy, xyxy, \text{ and } xyyx$.

The optical conductivities of gapped graphene under the linear dispersion approximation have been studied, and analytical expressions for them have been obtained.²⁴ For later use, we list the expressions in the clean limit. The linear conductivity is given by

$$\sigma_{gg}^{(1);xx}(\omega) = \frac{i\sigma_0}{\pi} \left[\frac{4E_c}{\hbar\omega} - \frac{4\Delta^2 + (\hbar\omega)^2}{(\hbar\omega)^2} \mathcal{G}(E_c; \hbar\omega) \right]. \quad (16)$$

Here $\sigma_0 = e^2/4\hbar$ is a universal conductivity, $E_c = \max\{|\Delta|, |\mu|\}$ is an effective gap parameter, and

$$\mathcal{G}(E_c; \hbar\omega) = \ln \left| \frac{\hbar\omega + 2E_c}{\hbar\omega - 2E_c} \right| + i\pi\theta(|\hbar\omega| - 2E_c), \quad (17)$$

with $\theta(x)$ being the usual step function. For the third order conductivity, the cyclic permutation symmetry on $\{a\omega_1, b\omega_2, c\omega_3\}$ of $\sigma_{gg}^{(3);dabc}(\omega_1, \omega_2, \omega_3)$ gives

$$\sigma_{gg}^{(3);xxyy}(\omega_1, \omega_2, \omega_3) = \sigma_{gg}^{(3);xyxy}(\omega_2, \omega_1, \omega_3) = \sigma_{gg}^{(3);xyyx}(\omega_2, \omega_3, \omega_1). \quad (18)$$

The third order conductivity is then

$$\begin{aligned} (i\sigma_3)^{-1} \sigma_{gg}^{(3);xxyy}(\omega_1, \omega_2, \omega_3) &= F_1(\Delta; \hbar\omega_1, \hbar\omega_2, \hbar\omega_3) \mathcal{G}(E_c; \hbar(\omega_1 + \omega_2 + \omega_3)) \\ &+ F_2(\Delta; \hbar\omega_1, \hbar\omega_2, \hbar\omega_3) \mathcal{G}(E_c; \hbar(\omega_2 + \omega_3)) \\ &+ F_3(\Delta; \hbar\omega_1, \hbar\omega_2, \hbar\omega_3) \mathcal{G}(E_c; \hbar(\omega_1 + \omega_3)) \\ &+ F_3(\Delta; \hbar\omega_1, \hbar\omega_3, \hbar\omega_2) \mathcal{G}(E_c; \hbar(\omega_1 + \omega_2)) \\ &+ F_4(\Delta; \hbar\omega_1, \hbar\omega_2, \hbar\omega_3) \mathcal{G}(E_c; \hbar\omega_1) \\ &+ F_5(\Delta; \hbar\omega_1, \hbar\omega_2, \hbar\omega_3) \mathcal{G}(E_c; \hbar\omega_2) \\ &+ F_5(\Delta; \hbar\omega_1, \hbar\omega_3, \hbar\omega_2) \mathcal{G}(E_c; \hbar\omega_3). \end{aligned} \quad (19)$$

with $\sigma_3 = \sigma_0(\hbar v_F e)^2/\pi$. The coefficients F_i are given by

$$F_i(\Delta; \epsilon_1, \epsilon_2, \epsilon_3) = \mathcal{F}_{i0}(\epsilon_1, \epsilon_2, \epsilon_3) + \Delta^2 \mathcal{F}_{i2}(\epsilon_1, \epsilon_2, \epsilon_3) + \Delta^4 \mathcal{F}_{i4}(\epsilon_1, \epsilon_2, \epsilon_3). \quad (20)$$

All the expressions of \mathcal{F}_{ij} are given in Appendix B. By setting $\Delta = 0$ we get the third order nonlinear conductivity for graphene as

$$\sigma_{gh}^{(3);xxyy}(\omega_1, \omega_2, \omega_3) = \sigma_{gg}^{(3);xxyy}(\omega_1, \omega_2, \omega_3) \Big|_{\Delta=0}. \quad (21)$$

We briefly discuss the asymptotic expression of these conductivities as $\Delta \rightarrow \infty$. In that limit $E_c = \max\{|\Delta|, |\mu|\} = \Delta$, and all involved photon energies satisfy $\hbar\omega_i/E_c \rightarrow 0$. As $\Delta \rightarrow \infty$, a direct expansion in the small quantities $\hbar\omega_i/\Delta$ gives

$$\sigma_{gg}^{(1);xx}(\omega) \rightarrow -i\sigma_0 \frac{4\hbar\omega}{3\pi\Delta}, \quad (22)$$

$$\sigma_{gg}^{(3);xxyy}(\omega_1, \omega_2, \omega_3) \rightarrow -i\sigma_3 \frac{2\hbar(\omega_1 + \omega_2 + \omega_3)}{45\Delta^5}. \quad (23)$$

The effective gap parameters E_c in Eq. (19) appear only in functions of \mathcal{G} , which determine possible resonances related to the interband transitions. Considering the photon energies involved in these functions, we note that the resonances can be associated with one-photon, two-photon, and three-photon processes. Both the one-photon and three-photon related resonances are similar to that of the linear conductivity, while the two-photon related resonance shows a different behavior. Since $F_2(\Delta; \epsilon_1, \epsilon_2, \epsilon_3) = 0$ for $\epsilon_2 + \epsilon_3 = 2\Delta$ and $F_3(\Delta; \epsilon_1, \epsilon_2, \epsilon_3) = 0$ for $\epsilon_1 + \epsilon_3 = 2\Delta$, the two-photon related resonances disappear for an undoped system.

III. CONDUCTIVITIES FOR THREE-DIMENSIONAL MASSLESS DIRAC FERMIONS

With the symmetry properties of the conductivities for 2D massive DF in one Dirac cone in hand, and with the analytic expressions of the conductivities for 2D gapped graphene already determined, we can now turn to the optical response of 3D massless DF. In this work, we focus on the optical response of an isotropic 3D Dirac cone, although more generally, of course, Dirac cones can be anisotropic; this is briefly discussed in Appendix A. For 3D massless DFs in a single isotropic Dirac cone the Hamiltonian⁴³ is

$$H_{3d}(\mathbf{k}) = \hbar v_F \mathbf{k} \cdot \boldsymbol{\sigma}, \quad (24)$$

where $\mathbf{k} = k_x \hat{\mathbf{x}} + k_y \hat{\mathbf{y}} + k_z \hat{\mathbf{z}}$ is a three dimensional wave vector. The two band energies are $\epsilon_{\pm k} = \pm \hbar v_F |\mathbf{k}|$, which touch at $\mathbf{k} = \mathbf{0}$, the Dirac point.

It is the conductivities following from this Hamiltonian in Eq. (24) that we study here, and we denote them by $\sigma_{3d}^{(1);da}(\omega)$ and $\sigma_{3d}^{(3);dabc}(\omega_1, \omega_2, \omega_3)$. The Hamiltonian $H_{3d}(\mathbf{k})$ is spherical symmetric, and so the only independent nonzero component of the linear conductivity is $\sigma_{3d}^{(1);xx}(\omega)$; for the third order conductivity, the independent nonzero components are the symmetric ones $\sigma_{3d}^{(3);xxyy}$, $\sigma_{3d}^{(3);xyxy}$, and $\sigma_{3d}^{(3);xyyx}$. All other components can be obtained

either by

$$\sigma_{3d}^{(3);xxxx} = \sigma_{3d}^{(3);xxyy} + \sigma_{3d}^{(3);xyxy} + \sigma_{3d}^{(3);yyxx}, \quad (25)$$

or by permutation of the directions $\{x, y, z\}$. Due to the cyclic permutation on $\{a\omega_1, b\omega_2, c\omega_3\}$ of $\sigma_{3d}^{(3);dabc}(\omega_1, \omega_2, \omega_3)$, and all nonzero component can be written in terms of $\sigma_{3d}^{(3);xxyy}(\omega_1, \omega_2, \omega_3)$, which we identify in the following.

The Hamiltonian for 3D massless DFs is connected to that of 2D massive DFs through the relation $H_{3d}(\boldsymbol{\kappa} + \Delta/(\hbar v_F)\hat{\mathbf{z}}) = H_{2d}(\boldsymbol{\kappa}, \Delta)$. In the calculation of both the linear and nonlinear conductivities in the independent particle approximation, the full response arises as the sum of the responses of each independent particles, identified initially by its \mathbf{k} . Thus the response of 3D massless DFs to electric fields in the x and y directions is equivalent to an ensemble of responses of 2D massive DFs with different gap parameters. In this manner the linear conductivity can be written as

$$\begin{aligned} \sigma_{3d}^{(1);xx} &= \int \frac{dk_z}{2\pi} \sigma_{2d}^{(1);xx}(\hbar v_F k_z) = \frac{1}{\pi \hbar v_F} \int_0^\infty d\Delta \sigma_{2d}^{(1);xx}(\Delta) \\ &= \frac{1}{4\pi \hbar v_F} \int_0^\infty d\Delta \sigma_{gg}^{(1);xx}(\Delta), \end{aligned} \quad (26)$$

where we have used $\sigma_{2d}^{(1);xx}(\Delta) = \sigma_{2d}^{(1);xx}(-\Delta)$ for the second equal sign and Eq. (14) for the third equal sign. Similarly we have

$$\sigma_{3d}^{(3);xxyy} = \frac{1}{4\pi \hbar v_F} \int_0^\infty d\Delta \sigma_{gg}^{(3);xxyy}(\Delta). \quad (27)$$

Once these are determined, all other nonvanishing components of the conductivities for 3D massless DFs follow from the symmetry properties of those tensors.

Using the results for the conductivity of gapped graphene in Eqs. (16) and (19), the integration can be done analytically, and the result is given in Appendix C. Because $\sigma_{gg}^{(1);xx} \propto \Delta^{-1}$ in Eq. (22), the integration in Eq. (26) diverges; this is associated with the assumption that the linear dispersion relation continues for all \mathbf{k} , no matter how large. Taking a cut-off energy E_A as the upper limit of the integration, to model the onset of more realistic band dispersion, the linear conductivity of three dimensional Dirac fermions in one cone is

$$\begin{aligned} \sigma_{3d}^{(1);xx}(\omega) &= \sigma_{3d,reg}^{(1);xx}(\omega) - \frac{ie^2 \hbar \omega}{12\pi^2 \hbar^2 v_F} \ln \frac{2E_A}{|\mu|}, \\ \sigma_{3d,reg}^{(1);xx}(\omega) &= \frac{ie^2}{24\pi \hbar^2 v_F} \frac{12|\mu|^2 - 5(\hbar\omega)^2 + 3(\hbar\omega)^2 \mathcal{Z}(|\mu|; \hbar\omega)}{3\pi \hbar \omega}, \end{aligned} \quad (28)$$

where the function \mathcal{Z} is given by

$$\begin{aligned}\mathcal{Z}(|\mu|; w) &= \ln |w^2 - 4\mu^2| - \ln \mu^2 - i\pi \text{sgn}(w)\theta(|w| - 2|\mu|) \\ &= \mathcal{T}\left(\frac{w}{|\mu|}\right),\end{aligned}\quad (29)$$

where

$$\mathcal{T}(x) = \ln |x^2 - 4| - i\pi \text{sgn}(x)\theta(x - 2), \quad (30)$$

with $\text{sgn}(x)$ the sign function. It is worth noting that E_A is not an cut-off energy for the energies of the DFs, but rather for the gap parameter; hence the expression in Eq. (28) is not exactly the same as those in literature that involve an energy cut-off.^{45,48,49} However, our result for the real part of the conductivity, which is the physically meaningful term, is consistent with earlier results in literature.

For the third order conductivity, the integration converges due to $\sigma^{(3);xyy} \propto \Delta^{-5}$ in Eq. (23), and the conductivity of 3D Dirac fermions is

$$\begin{aligned}\sigma_{3d}^{(3);xyy}(\omega_1, \omega_2, \omega_3) &= \frac{iv_F e^4}{16\pi^2} \left\{ \frac{8}{45\hbar^3 \omega_1 \omega_2 \omega_3} \right. \\ &\quad + \mathcal{C}_1(\hbar\omega_1, \hbar\omega_2, \hbar\omega_3) \mathcal{Z}(|\mu|; \hbar(\omega_1 + \omega_2 + \omega_3)) \\ &\quad + \mathcal{C}_2(\hbar\omega_1, \hbar\omega_2, \hbar\omega_3) \mathcal{Z}(|\mu|; \hbar(\omega_2 + \omega_3)) \\ &\quad + \mathcal{C}_3(\hbar\omega_1, \hbar\omega_2, \hbar\omega_3) \mathcal{Z}(|\mu|; \hbar(\omega_1 + \omega_3)) \\ &\quad + \mathcal{C}_3(\hbar\omega_1, \hbar\omega_3, \hbar\omega_2) \mathcal{Z}(|\mu|; \hbar(\omega_1 + \omega_2)) \\ &\quad + \mathcal{C}_4(\hbar\omega_1, \hbar\omega_2, \hbar\omega_3) \mathcal{Z}(|\mu|; \hbar\omega_1) \\ &\quad + \mathcal{C}_5(\hbar\omega_1, \hbar\omega_2, \hbar\omega_3) \mathcal{Z}(|\mu|; \hbar\omega_2) \\ &\quad \left. + \mathcal{C}_5(\hbar\omega_1, \hbar\omega_3, \hbar\omega_2) \mathcal{Z}(|\mu|; \hbar\omega_3) \right\},\end{aligned}\quad (31)$$

where \mathcal{C}_i is given by

$$\mathcal{C}_i(\hbar\omega_l, \hbar\omega_m, \hbar\omega_n) \mathcal{Z}(|\mu|; \hbar\omega) = \left[\sum_{j=0,2,4} \mathcal{F}_{ij}(\hbar\omega_l, \hbar\omega_m, \hbar\omega_n) \frac{(-\hbar\omega)^{j+1}}{2^{j+1}} \frac{1}{j+1} \right] \mathcal{Z}(|\mu|; \hbar\omega). \quad (32)$$

Note that the coefficients \mathcal{C}_i in $\sigma_{3d}^{(3);xyy}$ satisfy

$$\begin{aligned}\mathcal{C}_1(\hbar\omega_1, \hbar\omega_2, \hbar\omega_3) + \mathcal{C}_2(\hbar\omega_1, \hbar\omega_2, \hbar\omega_3) + \mathcal{C}_3(\hbar\omega_1, \hbar\omega_2, \hbar\omega_3) + \mathcal{C}_3(\hbar\omega_1, \hbar\omega_3, \hbar\omega_2) \\ + \mathcal{C}_4(\hbar\omega_1, \hbar\omega_2, \hbar\omega_3) + \mathcal{C}_5(\hbar\omega_1, \hbar\omega_2, \hbar\omega_3) + \mathcal{C}_5(\hbar\omega_1, \hbar\omega_3, \hbar\omega_2) = 0.\end{aligned}\quad (33)$$

IV. CONDUCTIVITIES FOR DIFFERENT OPTICAL PHENOMENA

Since 3D massless DFs form an isotropic system, the current density response can be written as

$$\begin{aligned} \mathbf{J}(t) = & \int \frac{d\omega}{2\pi} e^{-i\omega t} \sigma^{(1);xx}(\omega) \mathbf{E}_\omega \\ & + \int \frac{d\omega_1 d\omega_2 d\omega_3}{(2\pi)^3} e^{-i(\omega_1+\omega_2+\omega_3)t} \left[\sigma_{3d}^{(3);xyxy}(\omega_1, \omega_2, \omega_3) \mathbf{E}_{\omega_1} (\mathbf{E}_{\omega_2} \cdot \mathbf{E}_{\omega_3}) \right. \\ & \left. + \sigma_{3d}^{(3);xyxy}(\omega_1, \omega_2, \omega_3) \mathbf{E}_{\omega_2} (\mathbf{E}_{\omega_3} \cdot \mathbf{E}_{\omega_1}) + \sigma_{3d}^{(3);xyyx}(\omega_1, \omega_2, \omega_3) \mathbf{E}_{\omega_3} (\mathbf{E}_{\omega_1} \cdot \mathbf{E}_{\omega_2}) \right], \quad (34) \end{aligned}$$

where $\mathbf{E}_\omega = \int dt \mathbf{E}(t) e^{i\omega t}$ is the Fourier transform of the electric field. In this section we consider the nature of this response for different optical phenomena.

A. Several general properties of the conductivities

We begin by discussing some general properties of the expressions for the linear and third order conductivities in Eqs. (28) and (31).

1. For all the nonlinear phenomena we discuss, the third order conductivity of 3D massless DFs exhibits features very similar to that of graphene,^{11,12,24} as we show below, including the appearance of resonances and divergences. In 3D massless DFs the conductivities involve the function $\mathcal{Z}(|\mu|; \hbar\omega)$, instead of the function $\mathcal{G}(|\mu|; \hbar\omega)$ relevant for graphene. Both functions describe the interband optical transition, but they are weighted by different densities of states. However, there are always singularities at $|\hbar\omega| = 2|\mu|$, around which the real part diverges logarithmically and the imaginary part shows a step function. Similar to the frequency dependence of the nonlinear response of graphene, the third order conductivity of 3D massless DFs involves photon energies $\hbar\omega_i$, $\hbar\omega_i + \hbar\omega_j$, and $\hbar(\omega_1 + \omega_2 + \omega_3)$, which appear in the second argument of the function $\mathcal{Z}(|\mu|; \hbar\omega)$. Thus, when any of these energies matches $2|\mu|$, a resonant interband transition may appear. When any of these energies is zero, an intraband divergence may appear and lead to a divergent conductivity value in the clean limit at zero temperature.
2. Scaling all energies by the chemical potential, the third order conductivity can be

written as

$$\sigma_{3d}^{(3);dabc}(|\mu|; \omega_1, \omega_2, \omega_3) = \frac{v_F e^4}{16\pi^2 |\mu|^3} S_{3d}^{(3);dabc} \left(\frac{\hbar\omega_1}{|\mu|}, \frac{\hbar\omega_2}{|\mu|}, \frac{\hbar\omega_3}{|\mu|} \right), \quad (35)$$

where the dimensionless function $S_{3d}^{(3);dabc}$ can be obtained from $\sigma_{3d}^{(3);dabc}$. To better understand the third order optical response of 3D massless DFs, we can compare it to that of graphene.¹¹ If we introduce an effective bulk conductivity of graphene by associating a thickness $d_{\text{eff}} \approx 3.3 \text{ \AA}$ with a graphene sheet, that effective bulk third order conductivity $\sigma_{gh;eff}^{(3);dabc}$ can be obtained from Eq. (21) by $\sigma_{gh;eff}^{(3);dabc} = \sigma_{gh}^{(3);dabc} / d_{\text{eff}}$, and it can be written as

$$\sigma_{gh;eff}^{(3);dabc}(|\mu|; \omega_1, \omega_2, \omega_3) = \frac{\hbar v_F^2 e^4}{4\pi d_{\text{eff}} |\mu|^4} S_{gh}^{(3);dabc} \left(\frac{\hbar\omega_1}{|\mu|}, \frac{\hbar\omega_2}{|\mu|}, \frac{\hbar\omega_3}{|\mu|} \right), \quad (36)$$

where $S_{gh}^{(3);dabc}$ is a dimensionless function¹¹ that can be obtained from $\sigma_{gh}^{(3);dabc}$. Besides the different detailed structures given in the dimensionless functions $S_{3d}^{(3);dabc}$ and $S_{gh}^{(3);dabc}$, the two conductivities above also show a different dependence on the Fermi velocity v_F and the chemical potential $|\mu|$. Their ratio gives

$$\frac{\sigma_{3d}^{(3);xyyy}}{\sigma_{gh;eff}^{(3);xyyy}} = \frac{d_{\text{eff}} |\mu|}{4\pi \hbar v_F} \frac{S_{3d}^{(3);xyyy}}{S_{gh}^{(3);xyyy}}. \quad (37)$$

The prefactor is inversely proportional to the Fermi velocity v_F and proportional to the chemical potential $|\mu|$. By taking the Fermi velocity to be that of graphene ($v_F = 10^6 \text{ m/s}$), the prefactor is about 0.04 for $|\mu| = 1 \text{ eV}$. Therefore, the third optical conductivity of 3D massless DFs in one Dirac cone is about two orders of magnitude smaller than the corresponding effective bulk third order conductivity of graphene. Note that $\sigma_{3d}^{(3);dabc}$ is for one Dirac cone only; if there exists degeneracy g of the Dirac cones, the third order conductivity $\sigma_{3d}^{(3);dabc}$ is g times as large.

3. When all involved frequencies satisfy $\hbar\omega_i/|\mu| \ll 1$, the third order nonlinear response in a doped Dirac semimetal should be mostly due to the intraband transitions. This limit can be obtained by taking $\hbar\omega_i \rightarrow x\hbar\omega_i$ and $x \rightarrow 0$, and we find an approximate conductivity is given by

$$\sigma_{3d}^{(3);xyyy}(\omega_1, \omega_2, \omega_3) \approx \frac{iv_F e^4}{16\pi^2} \frac{8}{45\hbar^3 \omega_1 \omega_2 \omega_3}. \quad (38)$$

It is independent of the chemical potential $|\mu|$, showing a different dependence on that quantity than that of graphene ($\propto |\mu|^{-1}$). Comparing this conductivity to the effective bulk conductivity of graphene, we find

$$\frac{\sigma_{3d}^{(3);xyy}}{\sigma_{gh;eff}^{(3);xyy}} = \frac{4|\mu|d_{\text{eff}}}{15\pi\hbar v_F}. \quad (39)$$

Taking the Fermi velocity to be that of graphene ($v_F = 10^6$ m/s), for $|\mu| = 1$ eV, the ratio is about 0.042.

4. In the undoped limit as the chemical potential $\mu \rightarrow 0$, the conductivities depend only on the frequencies. In this limit, the third order conductivity of graphene is very simple:¹¹ $\sigma^{(3);xyy} \propto [(\omega_1 + \omega_2)(\omega_2 + \omega_3)(\omega_3 + \omega_1)(\omega_1 + \omega_2 + \omega_3)]^{-1}$. For 3D massless DFs, the expression for the third order conductivity in this limit is more complicated. Although the function $\mathcal{Z}(|\mu|; \hbar\omega)$ includes a term $\ln \mu^2$, it does not lead to any divergence because the term is cancelled out due to Eq. (33), thus the conductivity itself has no singularity at $|\mu| = 0$, and is well behaved as $\mu \rightarrow 0$.
5. Considering the dependence on the Fermi velocity v_F , the conductivities of graphene give $\sigma_{gh;eff}^{(n)} \propto v_F^{n-1}$, while those of 3D massless DFs give $\sigma_{3d}^{(n)} \propto v_F^{n-2}$. For graphene, the universal conductance appears in the linear optical response.⁵⁰ For Dirac fermions, the response independent of the material parameter should occur at second order, and in our simple model this is absent. But for Weyl semimetals, where inversion symmetry is broken, the universal optical response does appear in the circular photogalvanic effect.^{33,37}

B. Linear optical response

For 3D massless DFs, the cutoff energy appears only in the imaginary part of the linear conductivity. The real part in the clean limit is given by

$$\text{Re}[\sigma_{3d}^{(1);xx}(\omega)] = \frac{e^2\omega}{24\pi\hbar v_F} \theta(\hbar\omega - 2|\mu|), \quad (40)$$

which is proportional to the frequency ω . This leads to a frequency independent imaginary part of the susceptibility $\text{Im}[\chi(\omega)] = \text{Re}[\sigma_{3d}^{(1);xx}(\omega)]/(\omega\epsilon_0) = e^2/(24\pi\hbar v_F\epsilon_0)$ for $\hbar\omega > 2|\mu|$, which is inversely proportional to the Fermi velocity v_F . Again taking the Fermi velocity

to be the same as the value for graphene, $v_F = 10^6$ m/s, the absorption coefficient is $\text{Im}[\chi(\omega)] \approx 0.36$.

In the low frequency regime, the term involving the cutoff energy may contribute little due to its prefactor $\hbar\omega$, and the main contribution comes from the Drude term

$$\sigma_{3d}^{(1);xx}(\omega) \approx \frac{ie^2|\mu|^2}{6\pi^2\hbar^2v_F} \frac{1}{\hbar\omega}. \quad (41)$$

It is proportional to the square of the chemical potential $|\mu|^2$, following the dependence of the density of states. The term $\sigma_{3d,reg}^{(1);xx}(\omega)$ can be rewritten as

$$\sigma_{3d,reg}^{(1);xx}(\omega) = \frac{e^2|\mu|}{24\pi\hbar^2v_F} S_{3d}^{(1)}\left(\frac{\hbar\omega}{|\mu|}\right), \quad (42)$$

with a dimensionless function

$$S_{3d}^{(1)}(x) = \frac{i}{\pi} \frac{12 - 5x^2 + 3x^2\mathcal{T}(x)}{3x}. \quad (43)$$

Its real and imaginary parts are plotted in Fig. 1. Around $x = 2$, there appears a logarithmic divergence in its imaginary part and a step change in its real part. For $x > 2$ the real part is linearly dependent on x .

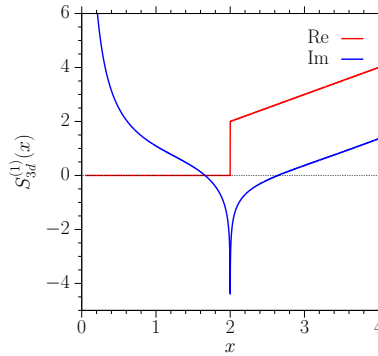


FIG. 1. The x dependence of $S_{3d}^{(1)}(x)$ in $0 < x < 4$.

C. Third harmonic generation

The third order conductivity for THG satisfies $\sigma_{3d}^{(3);xxyy} = \sigma_{3d}^{(3);xyxy} = \sigma_{3d}^{(3);xyyx} = \sigma_{3d}^{(3);xxxx}/3$. The quantity $S_{3d}^{(3);xxyy}(x, x, x)$ is given by

$$S_{3d}^{(3);xxyy}(x, x, x) = \frac{2i}{135x^3} [12 - 5\mathcal{T}(x) + 32\mathcal{T}(2x) - 27\mathcal{T}(3x)]. \quad (44)$$

Each \mathcal{T} term is associated with one optical transition involving photon energy $n\hbar\omega$ ($n = 1, 2$, or 3). Similar to the expression for the response tensor describing THG in graphene, the prefactors of these terms have different signs, indicating the existence of interference between these transitions. The real part is

$$\text{Re}[S_{3d}^{(3);xxyy}(x, x, x)] = \frac{2\pi\text{sgn}(x)}{135x^3} [-5\theta(|x| - 2) + 32\theta(2|x| - 2) - 27\theta(3|x| - 2)]. \quad (45)$$

For $x > 2$, $\text{Re}[S_{3d}^{(3)}(x, x, x)] = 0$ gives a complete cancellation due to interference. For graphene, the cancellation is not complete.^{8,11} In Fig. 2, we plot the spectra of $S_{3d}^{(3);xxyy}$ and

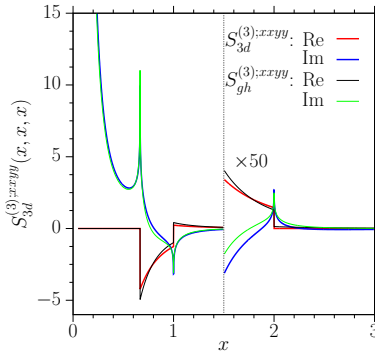


FIG. 2. The x dependence of $S_{3d}^{(3);xxyy}(x, x, x)$ and $S_{gh}^{(3);xxyy}(x, x, x)$. Values in the regime $x > 1.5$ are scaled by 50 times.

$S_{gh}^{(3);xxyy}$. They show very similar amplitudes and structures.

We close the summary of our results by presenting the conductivity in the limit of $\mu \rightarrow 0$. It corresponds to taking $x \rightarrow \infty$ in $S_{3d}^{(3);xxyy}(x, x, x)$; thus the real part is fully cancelled, and the imaginary part is given by

$$\sigma_{3d}^{(3);xxyy}(\omega, \omega, \omega)|_{\mu=0} = \frac{iv_F e^4 (6 + 32 \ln 2 - 27 \ln 3)}{540\pi^2 (\hbar\omega)^3}. \quad (46)$$

Finally we compare our results with those obtained in a velocity gauge using Floquet states by Zhang *et al.*⁴³ and Zhong *et al.*⁴⁴ At zero temperature, the real part of their results for one Dirac cone gives

$$\text{Re}[S_{3d}^{(3);xxyy}(x, x, x)]_{lit} = \frac{2\pi\text{sgn}(x)}{135x^3} [-4\theta(|x| - 2) + 16\theta(2|x| - 2) - 27\theta(3|x| - 2)], \quad (47)$$

with the imaginary part obtained using Kramers-Kronig relations.⁴³ The results differ from ours in the first two factors for one and two photon resonant processes, and the difference may arise from the choice of the velocity or length gauge to describe the light-matter interaction.

Considering the well-known problems that can result using the velocity gauge, a further investigation is required to clarify what causes the different results of these two methods.

D. The Kerr effect and two photon absorption

For a monochromatic laser beam, another important optical nonlinearity involves the corrections to the linear response due to the Kerr effect and two photon absorption, which are described by the tensor $\sigma_{3d}^{(3);dabc}(-\omega, \omega, \omega)$. For the frequency set $(-\omega, \omega, \omega)$, there are only two independent components $\sigma_{3d}^{(3);xxyy}(-\omega, \omega, \omega)$ and $\sigma_{3d}^{(3);xyyx}(-\omega, \omega, \omega) = \sigma_{3d}^{(3);xxyy}(-\omega, \omega, \omega)$. Intraband divergences exist for this third order conductivity, which are illustrated by

$$\begin{pmatrix} S_{3d}^{(3);xxyy}(-x, x + \delta_1, x + \delta_2) \\ S_{3d}^{(3);xyyx}(-x, x + \delta_1, x + \delta_2) \end{pmatrix} = \frac{4\pi \text{sgn}(x)\theta(x^2 - 4)}{45w} B_d(x; \delta_1, \delta_2) + B_n(x) + \dots \quad (48)$$

Here the first term indicates all the intraband divergences with respect to δ_1 and δ_2 , but they are nonzero only when one-photon absorption exists at $|x| > 2$, which is consistent with the general properties of intraband divergences.²⁴ The function B_d is given by

$$B_d(x; \delta_1, \delta_2) = \frac{\begin{bmatrix} -3 \\ 2 \end{bmatrix}}{\delta_1 \delta_2} + \frac{\begin{bmatrix} 4x + 3\delta_2 \\ -(x + 2\delta_2) \end{bmatrix}}{\delta_1(x + \delta_2)(2x + \delta_2)} + \frac{\begin{bmatrix} 9x + 3\delta_1 \\ -(x + 2\delta_1) \end{bmatrix}}{\delta_2(x + \delta_1)(2x + \delta_1)}. \quad (49)$$

The second term B_n is well behaved and given by

$$\begin{aligned} B_n(x) = \frac{1}{90x^3} & \left(\begin{bmatrix} -31 \\ 14 \end{bmatrix} \mathcal{T}(-x) + \begin{bmatrix} -65 \\ 50 \end{bmatrix} \mathcal{T}(x) + \begin{bmatrix} 96 \\ -64 \end{bmatrix} \mathcal{T}(2x) \right. \\ & \left. + x \begin{bmatrix} -52 \\ 8 \end{bmatrix} \frac{\partial \mathcal{T}(x)}{\partial x} + x^2 \begin{bmatrix} -12 \\ 8 \end{bmatrix} \frac{\partial^2 \mathcal{T}(x)}{\partial x^2} - 16 \begin{bmatrix} 1 \\ 1 \end{bmatrix} \right). \end{aligned} \quad (50)$$

In Fig. 3 we plot $S_{3d}^{(3);dabc}(-x, x, x)$ for $0 < x < 2$, and compare it with $S_{gh}^{(3);dabc}(-x, x, x)$. In general, both functions show very similar structures and amplitudes, except for two obvious differences: (1) $\text{Im}[S_{3d}^{(3);xxyy}]$ diverges to $-\infty$ as $x \rightarrow 2$, while $\text{Im}[S_{gh}^{(3);xxyy}]$ diverges to $+\infty$; (2) For graphene the real parts of these two components satisfy $\text{Re}[S_{gh}^{(3);xxyy}] = -\text{Re}[S_{3d}^{(3);xxyy}]$; however, for 3D massless DFs $S_{3d}^{(3);xxyy}$ this does not hold. For $x > 2$, the intraband divergences dominate, and in practice both the relaxation processes and pulse shape effects will determine the magnitude of the response. As a comparison, in the clean

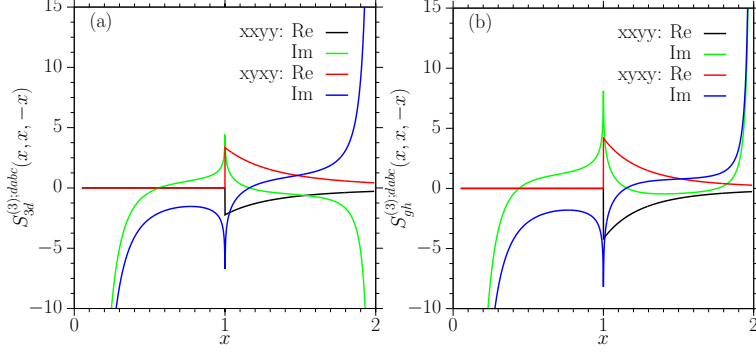


FIG. 3. The x dependence of (a) $S_{3d}^{(3);dabc}(x, x, -x)$ and (b) $S_{gh}^{(3);dabc}(x, x, -x)$ for the $xxyy$ and $xyxy$ components.

limit the results of Zhong *et al.*,⁴⁴ Zhang *et al.*,⁴³ and Ooi *et al.*^{42,45} give $\text{Re}[\sigma_{3d}^{(3);xxxx}] \propto \theta(\hbar\omega - 2|\mu|)$, which contains no two photon absorption.⁵¹ We are not sure whether or not such a difference occurs due to the different choices for the light-matter interaction.

Next we present our results for two photon carrier injection. When one-photon absorption is absent ($x < 2$), the two photon absorption coefficient can be calculated through $\xi_2^{abcd}(\omega) = 3(\hbar\omega)^{-1}\text{Re}[\sigma^{(3);abcd}(-\omega, \omega, \omega)]$.¹¹ It can be written as

$$\begin{pmatrix} \xi_2^{xyxy}(\omega) \\ \xi_2^{xyxy}(\omega) \end{pmatrix} = \frac{v_F e^4}{240\pi|\mu|^4} \text{sgn}(\omega) X \left(\frac{\hbar\omega}{|\mu|}; \frac{\hbar\delta_1}{|\mu|}, \frac{\hbar\delta_2}{|\mu|} \right), \quad (51)$$

with

$$X(x; \delta_1, \delta_2) = -\frac{4}{x^2} A_d(x; \delta_1, \delta_2) \theta(x^2 - 4) + \frac{1}{x^4} \begin{pmatrix} 48\theta(x^2 - 1) - 17\theta(x^2 - 4) \\ -32\theta(x^2 - 1) + 18\theta(x^2 - 4) \end{pmatrix}. \quad (52)$$

The first term comes from the intraband divergences, part of which enters in the second term giving contributions proportional to $\theta(x^2 - 4)$. The first term exists only in the presence of one-photon absorption ($x > 2$), and physically the divergences are induced by the stimulated Raman scattering process. For $1 < x < 2$ (*i.e.*, $|\mu| < \hbar\omega < 2|\mu|$), two photon absorption gives

$$\begin{pmatrix} \xi_2^{xyxy}(\omega) \\ \xi_2^{xyxy}(\omega) \end{pmatrix} = \frac{v_F e^4}{15\pi(\hbar\omega)^4} \begin{pmatrix} 3 \\ -2 \end{pmatrix}. \quad (53)$$

Compared to the results for graphene, the frequency dependence changes from ω^{-5} to ω^{-4} .

E. Parametric frequency conversion

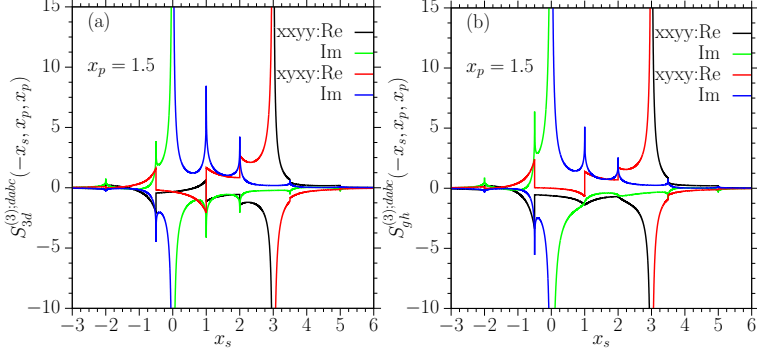


FIG. 4. The x_s dependence of the spectra for (a) $S_{3d}^{(3);dabc}(-x_s, x_p, x_p)$ for three dimension massless Dirac fermions and (b) $S_{gh}^{(3);dabc}(-x_s, x_p, x_p)$ for graphene. The pump frequency is chosen as $x_p = 1.5$.

When there are two laser beams, one with pump frequency ω_p and the second with signal frequency ω_s , a new frequency $2\omega_p - \omega_s$ can be generated through PFC; the current density responsible for it is determined by $\sigma_{3d}^{(3);dabc}(-\omega_s, \omega_p, \omega_p)$. For 3D massless DFs, this process has only two independent components: $\sigma_{3d}^{(3);xxyy}$ and $\sigma_{3d}^{(3);xyxy} = \sigma_{3d}^{(3);xyyx}$. Defining $x_{s,p} \equiv \hbar\omega_{s,p}/|\mu|$, the term $S_{3d}^{(3);dabc}(-x_s, x_p, x_p)$ shows interband divergences under the conditions $x_s = \pm 2$, $x_p = \pm 2$, $x_p = \pm 1$, $x_p - x_s = \pm 2$, or $2x_p - x_s = \pm 2$, and intraband divergences at $2x_p - x_s = 0$, $x_s = 0$. As an illustration, we fix $x_p = 1.5$ and show different components in Fig. 4. The possible divergences appear at $x_s = -2$, -0.5 , 1 , 3 , and 3.5 (interband), and at $x_s = 0$ and 5 (intraband). All these divergences exist for $S_{3d}^{(3);dabc}$, but two of these divergences – those at $x_s = 1$ and 2 – are removed for $S_{gh}^{(3);dabc}$. Both conductivities exhibit similar amplitudes and structures. For the intraband divergences, that at $x_s = 0$ is associated with a field/current induced second harmonic generation, and the other at $x_s = 2x_p$ corresponds to two-color CCI, which is discussed in the next section. Around these two divergences, the conductivities diverge as x_s^{-1} around $x_s \sim 0$, and $(x_s - 2x_p)^{-1}$ as $x_s \sim 2x_p$. Obviously, the spectra diverge much faster around intraband divergences than around interband divergences, where the divergences are logarithmic.

F. Two-color coherent current injection

The intraband divergences of $\sigma_{3d}^{(3);dabc}(-\omega, -\omega, 2\omega + \delta)$ as $\delta \rightarrow 0$ corresponds to a well known nonlinear phenomenon, two-color coherent current injection, in which a quasi-static current can be generated due to the interference of one-photon absorption and two-photon absorption processes. The divergence means that the current is continually injected, or

$$\frac{dJ^a(t)}{dt} = \eta_{3d}^{abcd}(\omega) E_{-\omega}^b E_{-\omega}^c E_{2\omega}^d + c.c. \quad (54)$$

with

$$\eta_{3d}^{abcd}(\omega) = \lim_{\delta \rightarrow 0} [-3i\delta \sigma_{3d}^{(3);abcd}(-\omega, -\omega, 2\omega + \delta)]. \quad (55)$$

After simple algebra, for $\omega > 0$ we get

$$\begin{pmatrix} \eta_{3d}^{xxyy}(\omega) \\ \eta_{3d}^{xyyx}(\omega) \end{pmatrix} = \frac{iv_F e^4}{60\pi(\hbar\omega)^2} \left[\begin{pmatrix} -6 \\ 4 \end{pmatrix} \theta(\hbar\omega - |\mu|) + \begin{pmatrix} 2 \\ -3 \end{pmatrix} \theta(\hbar\omega - 2|\mu|) \right]. \quad (56)$$

The term involving $\theta(\hbar\omega - |\mu|)$ is associated with the interference between the transition channels induced by a two-photon absorption ($\omega + \omega$) and a one-photon absorption (2ω), while the other term involving $\theta(\hbar\omega - 2|\mu|)$ is associated with the interference of stimulated electronic Raman scattering (for photon frequencies 2ω and $-\omega$) and one-photon absorption (ω). Compared to the injection in graphene, the injection coefficients in 3D massless DFs are proportional to $(\hbar\omega)^{-2}$, instead of $(\hbar\omega)^{-3}$ in graphene;¹¹ the relative amplitudes between different components are also different.

V. CONCLUSION AND DISCUSSION

We have calculated the linear and third order conductivities for a single Dirac cone of 3D massless Dirac fermions. In our simple model, we treat the light-matter interaction in the length gauge, in which the kind of unphysical divergences associated with band truncation that can appear in the velocity gauge do not arise. Analytic expressions for general input frequencies were obtained in the clean limit at zero temperature. Utilizing these expressions, we discussed in detail the frequency dependence of third harmonic generation, the Kerr effect and two photon absorption, parametric frequency conversion, and two-color coherent current injection. The dimension affects the optical response of Dirac fermions in several ways, and a

comparison between two and three dimensional massless Dirac fermions allows us to identify the following qualitative features: (1) the dependence on the Fermi velocity v_F , which is the relevant material parameter in these systems, changes from v_F^{n-1} in 2D to v_F^{n-2} in 3D for the n th order conductivity, (2) the chemical potential dependence of the third order conductivity changes from μ^{-1} to μ^0 for a lightly doped sample, (3) the frequency dependence of the two photon carrier injection changes from ω^{-5} to ω^{-4} , (4) the frequency dependence of two color current injection changes from ω^{-3} to ω^{-2} , and (5) for nonzero chemical potential, both frequency spectra show very similar structures in general, but their amplitude can differ up to two order of magnitude.

Although our results are obtained in the clean limit at zero temperature, they provide a general picture for third order response in three dimensional massless Dirac fermions, and they can be treated as a starting point for future study in nonlinear response of Dirac and Weyl semimetals.

Finally, we discuss the inclusion of phenomenological relaxation parameters and finite temperature, both of which are straightforward. For the third order conductivity of gapped graphene in our previous work,²⁴ the gap parameter appears in the conductivities as functions of $1/E_c^i$ ($i=1,3,5$), $\Delta^n \mathcal{G}(E_c; w)$, $\Delta^n \mathcal{H}(E_c; w) = \frac{\partial}{\partial w} [\Delta^n \mathcal{G}(E_c; w)]$, and $\Delta^n \mathcal{I}(E_c; w) = -\frac{\partial}{\partial w} [\Delta^n \mathcal{H}(E_c; w)]$ for $n = 0, 2, 4$. The integration of the latter two functions with respect to Δ can be derived from those for $\Delta^n \mathcal{G}(E_c; w)$. The integrations of $\int_0^{E_A} E_c^{-i} d\Delta$ can also be obtained easily. Therefore, the third order conductivity with finite phenomenological relaxation parameters can be obtained by replacing $\Delta^n \mathcal{G}(E_c; w) \rightarrow \mathcal{Y}_n(|\mu|; w)$, $\Delta^n \mathcal{H}(E_c; w) \rightarrow \frac{\partial}{\partial w} \mathcal{Y}_n(|\mu|; w)$, and $\Delta^n \mathcal{I}(E_c; w) \rightarrow -\frac{\partial^2}{\partial w^2} \mathcal{Y}_n(|\mu|; w)$, and leaving the divergent terms with respect to E_A in the integration of $\int_0^{E_A} E_c^{-i} d\Delta$. The complicated but analytic expressions could be evaluated numerically. Starting from the chemical potential dependence of the conductivity $\sigma_{3d}^{(1);xx}(|\mu|; \omega)$ and $\sigma_{3d}^{(3);xyyy}(|\mu|; \omega_1, \omega_2, \omega_3)$ at zero temperature, the corresponding dependence at finite temperature can be constructed using the technique presented earlier.¹² With this in hand, an investigation of the effects of the relaxation parameter and finite temperature on the optical conductivities of three dimensional Dirac fermions can be undertaken.

However, we want to emphasize that even with such a treatment of phenomenological relaxation parameters, and the consideration of finite temperature, a detailed comparison with experiments on materials exhibiting three dimensional massless Dirac fermions only

makes sense for low light frequencies, due to small energy range over which the assumption of a linear regime in the band dispersion is valid. More generally, realistic calculations based on full band structures will be required. Nonetheless, the study we have presented here will serve as a benchmark for identifying when those full band structure calculations show a significant difference from ideal Dirac fermion behavior.

ACKNOWLEDGMENTS

This work has been supported by K.C.Wong Education Foundation Grant No. GJTD-2018-08), Scientific research project of the Chinese Academy of Sciences Grant No. QYZDB-SSW-SYS038, National Natural Science Foundation of China Grant No. 11774340 and 61705227. S.W.W. is supported by the National Key Research and Development Program of China (Grant No 2019YFA0308404). J.E.S. is supported by the Natural Sciences and Engineering Research Council of Canada. J.L.C. acknowledges the support from “Xu Guang” Talent Program of CIOMP.

Appendix A: Comparing responses

We consider the relation between the optical conductivities of two different systems with Hamiltonians, $H^A(\mathbf{k})$ and $H^B(\mathbf{k})$, that are connected via a unitary matrix U and a real matrix R through

$$UH^A(R\mathbf{k})U^\dagger = H^B(\mathbf{k}). \quad (\text{A1})$$

The dynamics of these two systems can be described by density matrices $\rho_{\mathbf{k}}^A(t)$ and $\rho_{\mathbf{k}}^B(t)$. Under the application of electric field $\mathbf{E}(t)$, they satisfy the equation of motion¹¹

$$\hbar\partial_t\rho_{\mathbf{k}}^A(t) = -i[H^A(\mathbf{k}), \rho_{\mathbf{k}}^A(t)] + e\mathbf{E}(t) \cdot \nabla_{\mathbf{k}}\rho_{\mathbf{k}}^A(t), \quad (\text{A2})$$

$$\hbar\partial_t\rho_{\mathbf{k}}^B(t) = -i[H^B(\mathbf{k}), \rho_{\mathbf{k}}^B(t)] + e\mathbf{E}(t) \cdot \nabla_{\mathbf{k}}\rho_{\mathbf{k}}^B(t). \quad (\text{A3})$$

To clearly indicate the field that leads to the response, we denote the solutions of these two equations as $\rho_{\mathbf{k}}^{A/B}(t; \mathbf{E}(t))$. The current density responses are functionals of the field $\mathbf{E}(t)$,

and can be calculated as

$$\mathbf{J}^A(t; \mathbf{E}(t)) = -\frac{e}{\hbar} \sum_{\mathbf{k}} \text{Tr} [\rho_{\mathbf{k}}^A(t; \mathbf{E}(t)) \nabla_{\mathbf{k}} H^A(\mathbf{k})] . \quad (\text{A4})$$

$$\mathbf{J}^B(t; \mathbf{E}(t)) = -\frac{e}{\hbar} \sum_{\mathbf{k}} \text{Tr} [\rho_{\mathbf{k}}^B(t; \mathbf{E}(t)) \nabla_{\mathbf{k}} H^B(\mathbf{k})] . \quad (\text{A5})$$

Now we determine the connection between $\rho_{\mathbf{k}}^A(t; \mathbf{E}(t))$ and $\rho_{\mathbf{k}}^B(t; \mathbf{E}(t))$ induced by the relation in Eq. (A1). Considering a transformation

$$\bar{\rho}_{\mathbf{k}}(t) = U \rho_{R\mathbf{k}}^A(t; \mathbf{E}(t)) U^{-1} , \quad (\text{A6})$$

from Eq. (A2), the dynamics of $\bar{\rho}_{\mathbf{k}}(t)$ is

$$\hbar \partial_t \bar{\rho}_{\mathbf{k}}(t) = -i[U H^A(R\mathbf{k}) U^{-1}, \bar{\rho}_{\mathbf{k}}(t)] + e[R\mathbf{E}(t)] \cdot \nabla_{\mathbf{k}} \bar{\rho}_{\mathbf{k}}(t) . \quad (\text{A7})$$

Utilizing Eq. (A1) it is transformed into Eq. (A3), and we can find the solution is

$$\bar{\rho}_{\mathbf{k}}(t) = \rho_{\mathbf{k}}^B(t; R\mathbf{E}(t)) , \quad (\text{A8})$$

Then from Eq. (A6) the connection between $\rho_{\mathbf{k}}^A(t)$ and $\rho_{\mathbf{k}}^B(t)$ is

$$\rho_{\mathbf{k}}^B(t; R\mathbf{E}(t)) = U \rho_{R\mathbf{k}}^A(t; \mathbf{E}(t)) U^{-1} . \quad (\text{A9})$$

In Eq. (A5) by replacing $\mathbf{E}(t) \rightarrow R\mathbf{E}(t)$ and utilizing Eq. (A9) and then comparing to Eq. (A4), we get

$$\mathbf{J}^A(t; \mathbf{E}(t)) = |R| (R^T)^{-1} \mathbf{J}^B(t; R\mathbf{E}(t)) . \quad (\text{A10})$$

Note that for all of this analysis R is not limited to be a orthogonal matrix, and therefore such transformation can be used to connect the response of an anisotropic Dirac cone, *i.e.* $H(\mathbf{k}) = \hbar v_f \mathbf{k} \cdot R \cdot \boldsymbol{\sigma}$, to that of an isotropic cone $H(\mathbf{k}) = \hbar v_f \mathbf{k} \cdot \boldsymbol{\sigma}$.

For a weak electric field $\mathbf{E}(t)$, the induced current density can be expanded in a power series of this field, and the expansion coefficients are the conductivity tensors. As an example, if the matrix R corresponds to an orthogonal matrix $R^T = R^{-1}$, the linear conductivity and third order conductivity of these two systems satisfy

$$\sigma_A^{(1);da} = R^{dd'} R^{aa'} \sigma_B^{(1);d'a'} , \quad (\text{A11})$$

$$\sigma_A^{(3);dabc} = R^{dd'} R^{aa'} R^{bb'} R^{cc'} \sigma_B^{(3);d'a'b'c'} . \quad (\text{A12})$$

Appendix B: Expressions of \mathcal{F}_{ij} for gapped graphene

Using $\epsilon_{ij} = \epsilon_i + \epsilon_j$ and $\epsilon = \epsilon_1 + \epsilon_2 + \epsilon_3$, we write

$$\mathcal{F}_{ij}(\epsilon_1, \epsilon_2, \epsilon_3) = \frac{\overline{\mathcal{F}}_{ij}(\epsilon_1, \epsilon_2, \epsilon_3)}{6\epsilon_1^2\epsilon_2^2\epsilon_3^2\epsilon_{12}\epsilon_{23}\epsilon_{31}\epsilon}, \quad (\text{B1})$$

where $\overline{\mathcal{F}}_{ij}(\epsilon_1, \epsilon_2, \epsilon_3)$ are given by

$$\overline{\mathcal{F}}_{10}(\epsilon_1, \epsilon_2, \epsilon_3) = \epsilon^2 [3\epsilon_1^3\epsilon_{23} + (-\epsilon_2\epsilon_3 + 2\epsilon_1^2 - \epsilon_1\epsilon_{23})\epsilon_{23}^2 + \epsilon_1\epsilon_2\epsilon_3(2\epsilon_{23} - \epsilon_1)], \quad (\text{B2})$$

$$\overline{\mathcal{F}}_{12}(\epsilon_1, \epsilon_2, \epsilon_3) = -8 [3\epsilon_1^2\epsilon_2\epsilon_3 + \epsilon_1^3\epsilon_{23} - \epsilon_{23}^2(\epsilon_2\epsilon_3 + \epsilon_1\epsilon_{23})], \quad (\text{B3})$$

$$\overline{\mathcal{F}}_{14}(\epsilon_1, \epsilon_2, \epsilon_3) = -16(\epsilon_2\epsilon_3 + \epsilon_1\epsilon_{23}). \quad (\text{B4})$$

$$\overline{\mathcal{F}}_{20}(\epsilon_1, \epsilon_2, \epsilon_3) = \epsilon_{12}\epsilon_{13}\epsilon_{23}^4, \quad (\text{B5})$$

$$\overline{\mathcal{F}}_{22}(\epsilon_1, \epsilon_2, \epsilon_3) = -8\epsilon_{12}\epsilon_{13}\epsilon_{23}^2, \quad (\text{B6})$$

$$\overline{\mathcal{F}}_{24}(\epsilon_1, \epsilon_2, \epsilon_3) = 16\epsilon_{12}\epsilon_{13}. \quad (\text{B7})$$

$$\overline{\mathcal{F}}_{30}(\epsilon_1, \epsilon_2, \epsilon_3) = -\epsilon_{12}\epsilon_{13}^2\epsilon_{23} [3\epsilon_1^2 + 2\epsilon_1\epsilon_2 - 3\epsilon_2\epsilon_3 + (2\epsilon_1 - \epsilon_3)\epsilon_{23}], \quad (\text{B8})$$

$$\overline{\mathcal{F}}_{32}(\epsilon_1, \epsilon_2, \epsilon_3) = 8\epsilon_{12}(\epsilon_1 - \epsilon_3)\epsilon_{23}(\epsilon + \epsilon_2), \quad (\text{B9})$$

$$\overline{\mathcal{F}}_{34}(\epsilon_1, \epsilon_2, \epsilon_3) = 16\epsilon_{12}\epsilon_{23}. \quad (\text{B10})$$

$$\overline{\mathcal{F}}_{40}(\epsilon_1, \epsilon_2, \epsilon_3) = \epsilon_1^2 [\epsilon_2\epsilon_3(\epsilon + \epsilon_{23})^2 + \epsilon(\epsilon - \epsilon_{23})\epsilon_{23}(3\epsilon + \epsilon_{23})], \quad (\text{B11})$$

$$\overline{\mathcal{F}}_{42}(\epsilon_1, \epsilon_2, \epsilon_3) = -8 [\epsilon_3^3\epsilon_{23} - \epsilon\epsilon_{23}^3 + \epsilon_2\epsilon_3(-3\epsilon^2 + \epsilon_{23}^2)], \quad (\text{B12})$$

$$\overline{\mathcal{F}}_{44}(\epsilon_1, \epsilon_2, \epsilon_3) = -16(-\epsilon_2\epsilon_3 + \epsilon_{23}\epsilon). \quad (\text{B13})$$

$$\overline{\mathcal{F}}_{50}(\epsilon_1, \epsilon_2, \epsilon_3) = -\epsilon_2^2 [\epsilon\epsilon_1(\epsilon_{23} + \epsilon_3)^2 + \epsilon_2\epsilon_3\epsilon_{23}(\epsilon_{23} + 3\epsilon_3)], \quad (\text{B14})$$

$$\overline{\mathcal{F}}_{52}(\epsilon_1, \epsilon_2, \epsilon_3) = 8 (-\epsilon_3^3\epsilon_{23} + \epsilon_3\epsilon_{23}^3 - 3\epsilon_1\epsilon_3^2\epsilon + \epsilon_1\epsilon_{23}^2\epsilon), \quad (\text{B15})$$

$$\overline{\mathcal{F}}_{54}(\epsilon_1, \epsilon_2, \epsilon_3) = -16(\epsilon_3\epsilon_{23} + \epsilon_1\epsilon). \quad (\text{B16})$$

Appendix C: Conductivity for 3D Dirac Fermions

The linear conductivity and third order conductivity of three dimensional Dirac fermions are constructed from Eqs. (26) and (27), respectively. The upper limit of the integration is

infinity, and thus it is necessary to introduce a cutoff energy A to analyse the integration

$$I^{(n)}(A) = \frac{1}{4\pi\hbar v_F} \int_0^A d\Delta \sigma_{gg}^{(n)}(\Delta), \quad (\text{C1})$$

and then $\sigma_{3d}^{(n)} = \lim_{A \rightarrow \infty} I^{(n)}(A)$. As $\Delta \rightarrow \infty$, From Eqs. (22) and (23) we have $\sigma_{gg}^{(1);xx}(\Delta \rightarrow \infty) \rightarrow -4i\sigma_0\hbar\omega/(3\pi)\Delta^{-1}$ and $\sigma_{gg}^{(3);xyyy}(\Delta \rightarrow \infty) \sim \Delta^{-5}$. It is obvious that $I^{(1);xx}(A \rightarrow \infty)$ diverges as $\ln A$ and $I^{(3);xyyy}(A \rightarrow \infty)$ converges.

The Δ dependence in the conductivities of gapped graphene appears in Δ or $\Delta^n \mathcal{G}(E_c; w)$ for $n = 0, 2, 4$. By extending the definition of $\mathcal{G}(E_c; w)$ to a complex $w = w_r + iw_i$ we get

$$\mathcal{G}(E_c; w) = i\pi + \mathcal{L}(E_c; w) - \mathcal{L}(-E_c; w) \quad (\text{C2})$$

with

$$\mathcal{L}(x; w_r + iw_i) = \frac{1}{2} \ln [(w_r + 2x)^2 + w_i^2] - i \arctan \frac{w_r + 2x}{w_i}, \quad (\text{C3})$$

As $w_i \rightarrow 0^+$, it becomes

$$\mathcal{L}(x; w_r) = \ln |w_r + 2x| - i \frac{\pi}{2} \text{sgn}(w_r + 2x). \quad (\text{C4})$$

with $\text{sgn}(x)$ the sign function.

For the term $\Delta^n \mathcal{G}(E_c; w)$, the integration is

$$\begin{aligned} \int_0^{E_A} x^n \mathcal{G}(\max\{|\mu|, x\}; w) dx &= \int_0^{|\mu|} x^n \mathcal{G}(|\mu|; w) dx + \int_{|\mu|}^{E_A} x^n \mathcal{G}(x; w) dx \\ &= \frac{|\mu|^{n+1}}{n+1} \mathcal{G}(|\mu|; w) + \mathcal{K}_n(E_A; w) - \mathcal{K}_n(|\mu|; w), \end{aligned} \quad (\text{C5})$$

with

$$\mathcal{K}_n(x; w) = \frac{1}{n+1} [x^{n+1} \mathcal{G}(x; w) - \mathcal{Q}_n(x; w)], \quad (\text{C6})$$

$$\begin{aligned} \mathcal{Q}_n(x; w) &= \frac{(-w)^{n+1}}{2^{n+1}} [\mathcal{L}(x; w) + (-1)^n \mathcal{L}(-x; w)] \\ &+ \frac{1}{2^{n+1}} \sum_{m=1}^{n+1} C_{n+1}^m \frac{(-w)^{n+1-m}}{m} [(w+2x)^m - (-1)^{n+1} (w-2x)^m]. \end{aligned} \quad (\text{C7})$$

Taking $A \rightarrow \infty$, $\mathcal{K}_n(A; w)$ diverges as $\propto \ln(2E_A)$, E_A^2 , and E_A^4 for $n = 0, 2, 4$. We collect all divergent terms into $\mathcal{R}_n(A; w)$ and write $\mathcal{K}_n(E_A; w) = \overline{\mathcal{K}}_n(w) + \mathcal{R}_n(E_A; w)$ with

$$\overline{\mathcal{K}}_0(w) = 0, \quad \overline{\mathcal{K}}_2(w) = -\frac{1}{8}w^3, \quad \overline{\mathcal{K}}_4(w) = -\frac{5}{192}w^5. \quad (\text{C8})$$

Therefore the integration becomes

$$\int_0^{EA} x^n \mathcal{G}(\max\{|\mu|, x\}; w) dx = \mathcal{Y}_n(|\mu|; w) + \mathcal{R}_n(A; w), \quad (\text{C9})$$

with

$$\mathcal{Y}_n(|\mu|; w) = \overline{\mathcal{K}}_n(w) + \frac{1}{n+1} \mathcal{Q}_n(|\mu|; w) \quad (\text{C10})$$

Now we can construct the conductivity $\sigma_{3d}^{(n)}$ from that of $\sigma_{gg}^{(n)}$ by replacing $\Delta^n \mathcal{G}(E_c; w)$ with $\mathcal{Y}_n(|\mu|; w)$. For the linear conductivity $\sigma_{3d}^{(1);xx}(\omega)$, the divergent term can be obtained from Eq. (22) directly. Based on Eq. (19), in the clean limit the third order conductivity for Dirac fermions is

$$\begin{aligned} & \sigma_{3d}^{(3);xyxy}(|\mu|; \omega_1, \omega_2, \omega_3) \\ &= \frac{iv_F e^4}{16\pi^2} \sum_{j=0,2,4} \left\{ \mathcal{F}_{1j}(\hbar\omega_1, \hbar\omega_2, \hbar\omega_3) \mathcal{Y}_j(|\mu|; \hbar(\omega_1 + \omega_2 + \omega_3)) \right. \\ & \quad + \mathcal{F}_{2j}(\hbar\omega_1, \hbar\omega_2, \hbar\omega_3) \mathcal{Y}_j(|\mu|; \hbar(\omega_2 + \omega_3)) + \mathcal{F}_{3j}(\hbar\omega_1, \hbar\omega_2, \hbar\omega_3) \mathcal{Y}_j(|\mu|; \hbar(\omega_1 + \omega_3)) \\ & \quad + \mathcal{F}_{3j}(\hbar\omega_1, \hbar\omega_3, \hbar\omega_2) \mathcal{Y}_j(|\mu|; \hbar(\omega_1 + \omega_2)) + \mathcal{F}_{4j}(\hbar\omega_1, \hbar\omega_2, \hbar\omega_3) \mathcal{Y}_j(|\mu|; \hbar\omega_1) \\ & \quad \left. + \mathcal{F}_{5j}(\hbar\omega_1, \hbar\omega_2, \hbar\omega_3) \mathcal{Y}_j(|\mu|; \hbar\omega_2) + \mathcal{F}_{5j}(\hbar\omega_1, \hbar\omega_3, \hbar\omega_2) \mathcal{Y}_j(|\mu|; \hbar\omega_3) \right\}. \quad (\text{C11}) \end{aligned}$$

It can be simplified in terms of the function $\mathcal{L}(x; w) + \mathcal{L}(-x; w)$, and we then get the expression in Eq. (31).

* jlcheng@ciomp.ac.cn

¹ A. H. Castro Neto, F. Guinea, N. M. R. Peres, K. S. Novoselov, and A. K. Geim, *Rev. Mod. Phys.* **81**, 109 (2009).

² A. C. Ferrari, F. Bonaccorso, V. Fal'ko, K. S. Novoselov, S. Roche, P. Bøggild, S. Borini, F. H. L. Koppens, V. Palermo, N. Pugno, J. A. Garrido, R. Sordan, A. Bianco, L. Ballerini, M. Prato, E. Lidorikis, J. Kivioja, C. Marinelli, T. Ryhänen, A. Morpurgo, J. N. Coleman, V. Nicolosi, L. Colombo, A. Fert, M. Garcia-Hernandez, A. Bachtold, G. F. Schneider, F. Guinea, C. Dekker, M. Barbone, Z. Sun, C. Galiotis, A. N. Grigorenko, G. Konstantatos, A. Kis, M. Katsnelson, L. Vandersypen, A. Loiseau, V. Morandi, D. Neumaier, E. Treossi, V. Pellegrini, M. Polini, A. Tredicucci, G. M. Williams, B. H. Hong, J.-H. Ahn, J. M. Kim, H. Zirath, B. J. van Wees, H. van der Zant, L. Occhipinti, A. D. Matteo, I. A. Kinloch, T. Seyller, E. Quesnel, X. Feng,

- K. Teo, N. Rupesinghe, P. Hakonen, S. R. T. Neil, Q. Tannock, T. Löfwander, and J. Kinaret, *Nanoscale* **7**, 4598 (2015).
- ³ F. Bonaccorso, Z. Sun, T. Hasan, and A. C. Ferrari, *Nat. Photon.* **4**, 611 (2010).
- ⁴ M. Glazov and S. Ganichev, *Phys. Rep.* **535**, 101 (2014).
- ⁵ K. J. A. Ooi and D. T. H. Tan, *Proc. R. Soc. A* **473**, 20170433 (2017).
- ⁶ T. Gu, N. Petrone, J. F. McMillan, A. van der Zande, M. Yu, G. Q. Lo, D. L. Kwong, J. Hone, and C. W. Wong, *Nat. Photon.* **6**, 554 (2012).
- ⁷ N. Vermeulen, D. Castelló-Lurbe, M. Khoder, I. Pasternak, A. Krajewska, T. Ciuk, W. Strupinski, J. Cheng, H. Thienpont, and J. Van Erps, *Nat. Commun.* **9**, 2675 (2018).
- ⁸ T. Jiang, D. Huang, J. Cheng, X. Fan, Z. Zhang, Y. Shan, Y. Yi, Y. Dai, L. Shi, K. Liu, C. Zeng, J. Zi, J. E. Sipe, Y.-R. Shen, W.-T. Liu, and S. Wu, *Nat. Photon.* **12**, 430-436 (2018).
- ⁹ G. Soavi, G. Wang, H. Rostami, D. G. Purdie, D. De Fazio, T. Ma, B. Luo, J. Wang, A. K. Ott, D. Yoon, S. A. Bourelle, J. E. Muench, I. Goykhman, S. Dal Conte, M. Celebrano, A. Tomadin, M. Polini, G. Cerullo, and A. C. Ferrari, *Nat. Nano.* **13**, 583 (2018).
- ¹⁰ S. A. Mikhailov, *Europhys. Lett.* **79**, 27002 (2007).
- ¹¹ J. L. Cheng, N. Vermeulen, and J. E. Sipe, *New J. Phys.* **16**, 053014 (2014); **18**, 029501 (2016).
- ¹² J. L. Cheng, N. Vermeulen, and J. E. Sipe, *Phys. Rev. B* **91**, 235320 (2015); **93**, 039904 (2016).
- ¹³ J. L. Cheng, N. Vermeulen, and J. E. Sipe, *Phys. Rev. B* **92**, 235307 (2015).
- ¹⁴ S. A. Mikhailov, *Phys. Rev. B* **93**, 085403 (2016).
- ¹⁵ H. Rostami and M. Polini, *Phys. Rev. B* **93**, 161411(R) (2016).
- ¹⁶ V. Margulis, E. Muryumin, and E. Gaiduk, *Phys. Lett. A* **380**, 304-310 (2016).
- ¹⁷ F. Hipolito, D. Dimitrovski, and T. G. Pedersen, *Phys. Rev. B* **99**, 195407 (2019).
- ¹⁸ B. Semnani, R. Jago, S. Safavi-Naeini, H. Majedi, E. Malic, and P. Tassin, *2D Mater.* **6**, 031003 (2019).
- ¹⁹ H. Rostami, M. I. Katsnelson, and M. Polini, *Phys. Rev. B* **95**, 035416 (2017).
- ²⁰ H. K. Avetissian and G. F. Mkrtchian, *Phys. Rev. B* **97**, 115454 (2018).
- ²¹ J. L. Cheng, J. E. Sipe, and C. Guo, *Phys. Rev. B* **100**, 245433 (2019).
- ²² S. A. Jafari, *J. Phys. Condens. Matter* **24**, 205802 (2012).
- ²³ J. L. Cheng and C. Guo, *Phys. Rev. B* **97**, 125417 (2018).
- ²⁴ J. L. Cheng, J. E. Sipe, S. W. Wu, and C. Guo, *APL Photonics* **4**, 034201 (2019).
- ²⁵ S. M. Young, S. Zaheer, J. C. Y. Teo, C. L. Kane, E. J. Mele, and A. M. Rappe, *Phys. Rev.*

- Lett. **108**, 140405 (2012).
- ²⁶ J. Ma, K. Deng, L. Zheng, S. Wu, Z. Liu, S. Zhou, and D. Sun, *2D Materials* **6**, 032001 (2019).
- ²⁷ A. Burkov, *Annu. Rev. Condens. Matter Phys* **9**, 359 (2018).
- ²⁸ H. Gao, J. W. Venderbos, Y. Kim, and A. M. Rappe, *Annu. Rev. Mater. Res.* **49**, 153 (2019).
- ²⁹ S. Jia, S.-Y. Xu, and M. Z. Hasan, *Nat. Mater.* **15**, 1140 (2016).
- ³⁰ S. Rao, *arXiv* (2016), arXiv:1603.02821.
- ³¹ B. Yan and C. Felser, *Annu. Rev. Condens. Matter Phys* **8**, 337 (2017).
- ³² S. A. Yang, *SPIN* **06**, 1640003 (2016).
- ³³ J. E. Moore, *Natl. Sci. Rev.* **6**, 206 (2018).
- ³⁴ Q. Ma, S.-Y. Xu, C.-K. Chan, C.-L. Zhang, G. Chang, Y. Lin, W. Xie, T. Palacios, H. Lin, S. Jia, P. A. Lee, P. Jarillo-Herrero, and N. Gedik, *Nat. Phys.* **13**, 842 (2017).
- ³⁵ Q. Ma, S.-Y. Xu, H. Shen, D. MacNeill, V. Fatemi, T.-R. Chang, A. M. M. Valdivia, S. Wu, Z. Du, C.-H. Hsu, S. Fang, Q. D. Gibson, K. Watanabe, T. Taniguchi, R. J. Cava, E. Kaxiras, H.-Z. Lu, H. Lin, L. Fu, N. Gedik, and P. Jarillo-Herrero, *Nature* **565**, 337 (2018).
- ³⁶ S. Chi, Z. Li, H. Yu, G. Wang, S. Wang, H. Zhang, and J. Wang, *Ann. Phys.* **529**, 1600359 (2017).
- ³⁷ F. de Juan, A. G. Grushin, T. Morimoto, and J. E. Moore, *Nat. Commun.* **8**, 15995 (2017).
- ³⁸ I. Sodemann and L. Fu, *Phys. Rev. Lett.* **115**, 216806 (2015).
- ³⁹ M. M. Vazifteh and M. Franz, *Phys. Rev. Lett.* **111**, 027201 (2013).
- ⁴⁰ X. Yang, K. Burch, and Y. Ran, “Divergent bulk photovoltaic effect in weyl semimetals,” (2017).
- ⁴¹ J. Ma, Q. Gu, Y. Liu, J. Lai, P. Yu, X. Zhuo, Z. Liu, J.-H. Chen, J. Feng, and D. Sun, *Nat. Mater.* **18**, 476 (2019).
- ⁴² K. J. A. Ooi, Y. S. Ang, Q. Zhai, D. T. H. Tan, L. K. Ang, and C. K. Ong, *APL Photonics* **4**, 034402 (2019).
- ⁴³ T. Zhang, K. J. A. Ooi, W. Chen, L. K. Ang, and Y. S. Ang, *Opt. Express* **27**, 38270 (2019).
- ⁴⁴ Y. Zhong, W. Feng, Z. Liu, C. Zhang, and J. C. Cao, *Phys. B* **555**, 81 (2019).
- ⁴⁵ K. J. Ooi, Y. Ang, Q. Zhai, X. Sun, P. Xing, C. Ong, L. Ang, and D. T. Tan, *Opt. Commun.* **462**, 125319 (2020).
- ⁴⁶ J. E. Sipe and E. Ghahramani, *Phys. Rev. B* **48**, 11705 (1993).
- ⁴⁷ A. Taghizadeh, F. Hipolito, and T. G. Pedersen, *Phys. Rev. B* **96**, 195413 (2017).

⁴⁸ O. V. Kotov and Y. E. Lozovik, Phys. Rev. B **93**, 235417 (2016).

⁴⁹ K. Sonowal, A. Singh, and A. Agarwal, Phys. Rev. B **100**, 085436 (2019).

⁵⁰ R. R. Nair, P. Blake, A. N. Grigorenko, K. S. Novoselov, T. J. Booth, T. Stauber, N. M. R. Peres, and A. K. Geim, Science **320**, 1308 (2008).

⁵¹ The results in Ref. [44] have an obvious typo, as a comparison with those in Ref. [43].